An ab Initio Molecular Orbital and Dynamics Study on Penning Ionization of Ar with He Metastables(He*(2^1S,2^3S)) into the Spin−Orbit $Ar^+(^2P_{3/2},^2P_{1/2})$ States

Toshimasa Ishida*

Applied Sciences, Faculty of Engineering, Shizuoka University, Johoku, Hamamatsu, 432-8561 Japan

Hideki Katagiri

National Institute of Advanced Industrial Science and Technology, 1-1-4 Umezono, Tsukuba, Ibaraki, 305-8568 Japan

Received: April 12, 2001; In Final Form: August 8, 2001

The Penning ionization Ar + He*(2^1S,2^3S) → $Ar^+(^2P_{3/2},^2P_{1/2})$ + He + e^- is investigated with ab initio and chemical reaction dynamics calculations. Ab initio molecular orbital calculations have been carried out to obtain resonance potential energy curves and partial widths for each spin−orbit ionized state. The result is compared with optical potentials obtained from experiments. The total widths are not well described by single-exponential functions both for the singlet and triplet entrance channels. This indicates that a more flexible functional form should be used to obtain the imaginary part of an optical potential. The total ionization cross sections are calculated by quasiclassical trajectory as well as quantum dynamics in the collision energy range of 0.05−1 eV. The calculations show that the ratio of the cross section for the $^2P_{3/2}$ ionized state to that for the $^2P_{1/2}$ state increases with collision energy, in agreement with experimental results. It is found that the sum of the partial ionization cross sections significantly deviates from the total ionization cross section at higher collision energies in quantum dynamics calculations. One should be cautious for the application of quantum dynamics treatment to treat partial ionization in particular at higher energies. Differential cross sections are also calculated by a quantum-dynamics scheme.

1. Introduction

Atoms and molecules in superexcited states of the first kind can autoionize through configuration interaction with ionized state, in which the superexcited states are embedded. Penning ionization[1] and associative ionization are two examples of the autoionization.[2] The superexcited He* can cause an atom or a molecule to ionize during collision

$$M + He^* \rightarrow M^+ + He + e^- \quad (1)$$

where M is an atom or a molecule except for He and Ne, because the excitation energies of He*(2^1S, 20.616 eV) and He*-(2^3S, 19.820 eV) are larger than the first ionization energy. In the present paper, we study the collision with Ar, ionization energies of which are 15.759 eV($^2P_{3/2}$) and 15.937 eV($^2P_{1/2}$):[3,4]

$$Ar + He^*(2^1S) \rightarrow Ar^+(^2P_{3/2},^2P_{1/2}) + He + e^- \quad (2)$$

and

$$Ar + He^*(2^3S) \rightarrow Ar^+(^2P_{3/2},^2P_{1/2}) + He + e^- \quad (3)$$

The collision of He* with Ar has been investigated experimentally by many researchers. Absolute total ionization cross sections, quenching rate constants, energy dependence of cross sections, and relative electronic state populations have been obtained using flowing afterglow, static afterglow, beam-gas, crossed-beam, and electron spectroscopy techniques.[5−7] Recently, Longley et al. and Ohno et al. measured collision energy dependence of Penning ionization electron spectra (PIES).[8,9] Longley and Siska measured angle-energy distributions of Penning ions using crossed molecular beams.[10] Feltgen et al. carried out a measurement of the collision energy dependence in the energy range of 0.003 to 6 eV.[11] Siddiqui et al. investigated the van der Waals molecule Ar_2.[12]

The resonant potential V and width Γ, which are the real and imaginary parts of the optical potential, have been obtained with fitting parameters from experiments by several groups for the singlet[11,13−15] and the triplet processes.[11,16−21] However, there is no direct procedure to date from an experiment to obtain a complex potential to our knowledge. This is quite different from the situation that an usual potential energy curve is obtained from an experiment of vibration−rotational spectroscopy by the Rydberg−Klein−Rees method.[22−25] Therefore, the determination of the optical potential from experiments suffers from ambiguity. Thus, ab initio determination of the potentials and the widths is necessary to clarify the ionization mechanism.

We have been studying Penning ionization reactions of molecular targets which yield several ionized states. We have carried out ab initio molecular orbital calculations[26,27] and classical and quantum dynamics calculations on the bases of ab initio optical potentials.[28−30] We already carried out an ab initio calculation and a classical trajectory calculations for the triplet system and reproduced the increase of the ratio of the cross section for the $^2P_{3/2}$ state to that for the $^2P_{1/2}$state with the energy.[31] In this paper, we calculate the Ar−He*(2^1S) and Ar−He*(2^3S) ionization and compare the results with experiments.

* To whom correspondence should be addressed. Email: ishida-t@eng.shizuoka.ac.jp. Fax: +81-54-478-1293.

10.1021/jp011395r CCC: $20.00
Published on Web 09/19/2001

2. Calculations

2.1. Ab Initio Calculations. The entrance channel of Penning ionization is embedded in ionization continua, so that we use an optical potential. The entrance potential $V(R)$ and the width $\Gamma(R)$ are the real and imaginary parts of the optical potential $V^*(R)$:

$$V^*(R) = V(R) - \frac{1}{2} i\Gamma(R) \tag{4}$$

where R is an internuclear distance.

$\Gamma(R)$ is the sum of the partial widths $\Gamma^{(i)}(R)$:

$$\Gamma(R) = \sum_i \Gamma^{(i)}(R) \tag{5}$$

where i denotes an individual ionized state. In the present study, the real part V is the resonance potential for Ar* + He. The V and $\Gamma^{(i)}$ are obtained from ab initio calculations based on the Feshbach projection operator method.[32,33] In the Feshbach projection operator method, we divide the CI space into a space to describe resonance state and spaces for ionized states and an ejected electron. Ionization occurs through configuration interaction between the resonance state and ionized states. We define the projection operators $P^{(i)}$ to obtain the latter spaces:

$$P^{(i)} = \sum_{j=1}^{n} |\chi_j^{(i)}\rangle \langle \chi_j^{(i)}| \tag{6}$$

and

$$\chi_j^{(i)} = A(\Psi_+^{(i)} \phi_j), \quad (j = 1, ..., n) \tag{7}$$

where $\Psi_+^{(i)}$ is the ith ionized state for $(Ar-He)^+$, ϕ_j is an (square integrable) orbital to describe an ejected electron, and A is the antisymmetrizer. We see later that ϕ_j is approximated by the projection of a Coulomb function onto a (square integrable) vacant orbital. The n is the number of orbitals to expand an ejected electron. Thus, $P^{(i)}$ is a projection operator onto one of continuum states correlated asymptotically to $Ar^+ + He + e^-$. We approximated $\Psi_+^{(i)}$ with a single Slater determinant. Molecular orbitals for a CI calculation were determined by a multiconfiguration self-consistent field calculation (MCSCF). The supplementary projection operator Q for the resonance state is defined as

$$Q = 1 - \sum_{i=1}^{N_{ion}} P^{(i)} \tag{8}$$

where N_{ion} is the number of relevant ionized states. In this case, $N_{ion} = 6$ with the spin−orbit coupling. A resonance state occurs at energy $E_r + \Delta$, where E_r is an eigenvalue of QHQ with eigenvector Ψ_r and the small shift Δ was neglected in the present study as usual. The width $\Gamma^{(i)}$ of the resonance state for each ionization is

$$\Gamma^{(i)} = 2\pi\rho^{(i)} | < P^{(i)}\chi^{(i)}| P^{(i)}HQ|\Psi_r > |^2 \tag{9}$$

where $\rho^{(i)}$ is the density of states for the ith ionization, and $\chi^{(i)}$ is the wave function for the ith final state (the ionized state plus a continuum electron). We approximate a released electron with a Coulomb function $\phi^{c(i)}$and expand in terms of partial waves:

$$P^{(i)}\chi^{(i)} \simeq A(\Psi_+^{(i)} \phi^{c(i)}) = \sum_{lm} A(\Psi_+^{(i)} \phi_{lm}^{c(i)}) \tag{10}$$

and

$$\phi_{lm}^{c(i)}(\boldsymbol{r}) = F_l^{(i)}(-1/k^{(i)}, k^{(i)}r) Y_l^m(\hat{r})/r \tag{11}$$

where $F_l^{(i)}$ is the radial Coulomb wave function for the electron which is released in the ionization into the ith state, $k^{(i)}$ is the wavenumber of a released electron, $\hat{r}$ is a unit vector for r, and $Y_l^m(\hat{r})$ is a spherical harmonic function. When the Coulomb wave function is used for a released electron, $2\pi\rho^{(i)} = 4/k^{(i)}$. Furthermore, we approximate $\phi_{lm}^{(i)}$ in the following manner:

$$\phi_{lm}^{c(i)} \simeq \sum_j |\phi_j\rangle \langle \phi_j|\phi_{lm}^{c(i)}\rangle \tag{12}$$

Thus, $\Gamma^{(i)}$ is expressed by the configuration interaction matrix elements and the overlap of the continuum orbital with usual square integrable molecular orbitals. Coulomb functions were employed to express ejected electrons, and the partial waves of the functions were expanded by the vacant orbitals. The center of the Coulomb functions was located on the Ar^+ atom. The overlap integrals in eq 12 used to express expansion coefficients were evaluated by numerical integration. We used the double-exponential function formula by Takahashi and Mori[34] for the radial part, and the Gauss−Legendre[35] and the trapezoidal formula were used for the angular parts.

The basis set employed was a triple-ζ plus polarization (TZP) class set augmented with diffuse 2s2p functions on the He atom to describe the 2s orbital of He. We performed averaged MCSCF calculations for three ionized states of $(Ar-He)^+$ that correlated asymptotically with the ^2P state without the spin−orbit interaction. Each ionized state was described by one configuration. The molecular orbitals determined by the MCSCF calculation were used as a basis for a SDCI (single- and double-substitution configuration interaction) calculation. We used the Ar−He(1s2s) configuration as the reference of the SDCI calculations. Twenty vacant orbitals were included in the SDCI space. The dimensions of CI matrices generated were 17 969 for the singlet state and 26 610 for the triplet state. Thus, the resonance state is described by 17 909 ($17969 - 3 \times 20$) and 26 550 ($26610 - 3 \times 20$) CSFs without spin−orbit interaction, for the singlet and triplet states.

Ionized spin−orbit states were determined by the CI calculations for six spin−orbit ionized states with the Breit−Pauli Hamiltonian.[36] Widths for spin−orbit states are evaluated from the projection of spin-free states.

The codes for the Feshbach projection operator calculations as well as for spin−orbit CI calculations were added to quantum chemistry program HONDO7 by Dupuis et al.[37] Spin−orbit integrals were obtained based on the method that King and Furlani proposed.[36] Their method uses the second derivatives of one-electron and two-electron integrals. The Hessian calculation portion of the HONDO7 program was utilized to obtain relevant integrals.

2.2. Classical and Quantum Mechanical Calculations for Dynamics. Quasiclassical and quantum mechanical calculations on the potential curve for V and the widths $\Gamma^{(i)}$ were carried out on a cubic spline fit to the points from ab initio calculations. The classical equations of motion were integrated by the fourth order Adams−Moulton scheme,[38] which was initiated by the fourth-order Runge−Kutta method.[35] The time step used was 1.0×10^{-16} s. Total and partial ionization probabilities for each time step were evaluated from energy widths, and accumulated to yield the probabilities for one trajectory. This is based on

classical formulas.[39,40] and we call the "probability-accumulating trajectory (PAT) method".[30]

The impact parameter is $b = (l + 1/2)/k$, where l is an angular momentum quantum number and k is an initial wavenumber of the particle with the reduced mass μ of the system. The initial separation between He and Ar is 15 Å, which accordingly determines the largest value of l. The total and partial ionization probability into the ith ionized state for a given l are expressed by

$$P_l = 1 - \exp[-\int_{-\infty}^{\infty} dt W(t)] \tag{13}$$

and

$$P_l^{(i)} = \int_{-\infty}^{\infty} dt W^i(t) \exp[-\int_{-\infty}^{t} dt' W(t')] \tag{14}$$

where $W(t) = \Gamma(R)/\hbar$ and $W^i(t) = \Gamma^{(i)}(R)/\hbar$ are the rates of total and partial ionizations. The total and partial cross sections are given by

$$\sigma^{\text{tot}} = \frac{\pi}{k^2} \sum_{l=0}^{l_{\max}} (2l+1) P_l \tag{15}$$

and

$$\sigma^{(i)} = \frac{\pi}{k^2} \sum_{l=0}^{l_{\max}} (2l+1) P_l^{(i)} \tag{16}$$

It can be shown in these formulas that the total ionization cross section is equal to the sum of the partial ionization cross sections. Calculations using optical potentials determined from experiments by other authors were also performed in the same scheme for comparison.

Quantum-dynamics calculations for total and partial cross sections were carried out following the method of Cohen and Lane.[41] The form of the Schrödinger equation is given by

$$\left[-\frac{1}{2\mu_{\text{Ar-He}}} \nabla_R^2 + V^*(R) - E\right] \psi(R) = 0 \tag{17}$$

where $\psi(R)$ is the wave function describing the relative motion of the He and Ar species and V^* is given by eq 4. If $\psi(R)$ is expanded as follows,

$$\psi(R) = \frac{1}{R} \sum_{l=0}^{\infty} u_l(R) P_l(\cos\theta) \tag{18}$$

where $P_l(\cos\theta)$ is a Legendre polynomial. The radial equation then becomes

$$\left(\frac{d^2}{dR^2} - \frac{l\,(l+1)}{R^2} + 2\mu_{\text{Ar-He}}[E - V^*(R)]\right) u_l(R) = 0 \tag{19}$$

Equation 19 was solved using Johnson's log-derivative method.[42] The integration was done up to the distance of 15 Å. This method yields the reaction matrix **K**. The original method was modified to allow the potentials and radial wave functions to be complex. The partitioning of the equation into the real and imaginary parts was not done. The resultant reaction matrix **K** and scattering matrix S were therefore also complex. (In this case, both **K** and **S** are 1×1 matrices.) The ionization cross section for the lth partial wave is given by

$$\sigma_l = \frac{\pi}{k^2} (2l+1)(1 - |S_l|^2) \tag{20}$$

where $S_l = \exp(2i\delta_l)$ and δ_l is a phase shift.

Since the potential V^* is complex, δ_l is also complex. If we define η_l to be the imaginary part of the phase shift, ionization probability P_l for the lth partial wave is given by

$$P_l = 1 - |S_l|^2 = 1 - \exp(-4\eta_l) \tag{21}$$

The (total) ionization cross section is given by

$$\sigma^{\text{tot}} = \sum_l \sigma_l \tag{22}$$

For the partial ionization into the ith ionized state, similar quantities $\sigma^{(i)}$can be defined,

$$\sigma^{(i)} = \sum_l \sigma_l^{(i)} \tag{23}$$

but the sum of (partial) ionization cross section into individual ionized states is not equal to the total ionization in this treatment

$$\sigma^{\text{tot}} \neq \sum_l \sigma^{(i)} \tag{24}$$

because the nonlinearity of $\exp(-4\eta_l)$.[8,30]

Using **S** matrices, a differential center-of-mass cross section $I(\theta)$ is calculated by scattering amplitude:

$$f(\theta) = \frac{1}{2ik} \sum_{l=0}^{\infty} (2l+1)(S_l - 1) P_l(\cos\theta) \tag{25}$$

and

$$I(\theta) = |f(\theta)|^2 \tag{26}$$

3. Optical Potentials and Ionized State Potential

3.1. Real Parts of Optical Potentials. Figure 1 shows the calculated real part potential curve V for the Ar−He* ionization with the curves obtained from differential scattering experiments.

For the singlet state, the curves determined by Martin et al.,[13] Haberland and Schmidt,[14] and Brutschy et al.[15] are included in Figure 1a. The real part of the optical potential by Martin et al. has a shoulder at $r = 3.2$ Å and $V = 26$ meV. The shoulder was qualitatively reproduced, but occurred at a higher energy of $V = 200$ meV at $r = 2.5$ Å. This situation was also found in the N_2−He*(2^3S) system,[26,28] which leads to ionization cross sections than smaller than experimental ones, as discussed later.

The present singlet real-part potential does not reveal an intermediate maximum. There have been arguments about the existence of an intermediate maximum in the real part of potential and whether the imaginary part is in a single-exponential form mainly between Freiburg group and Siska's group.[10,13−15,43−47] The unusual structure of the present real part potential is much more enhanced than the other potentials, so that it is difficult to discuss whether the structure of the potential appears at or below 0.05 eV. However, as shown below, the imaginary part of the potential cannot be described by a single-exponential function. Thus, it would not be reasonable to argue on the basis of the idea that the imaginary part of the potential be a single-exponential function.

The present potential does not show a potential minimum while other potentials obtained by experiments show very

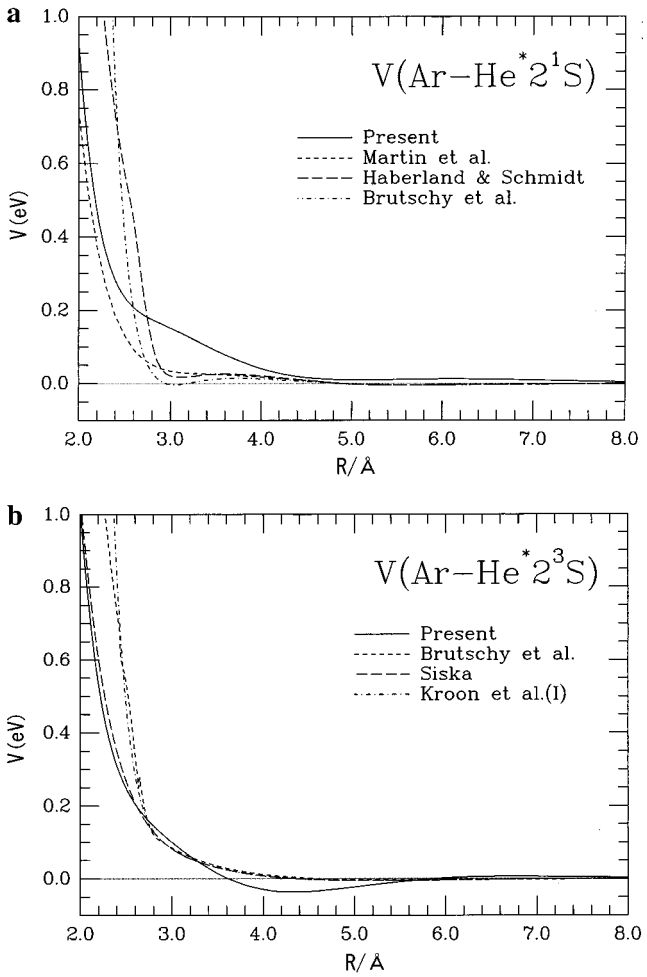

Figure 1. The potential energy curve of the entrance channel. (a) Ar + He*(2^1S) and (b) Ar + He*(2^3S). The curves obtained from differential scattering experiments by Martin et al.[13] and Haberland and Smith;[14] by Brutschy et al.[15] for the singlet in part a; and by Brutschy et al.,[17] Siska,[18] and Kroon et al.[21] for the triplet in part b are also shown.

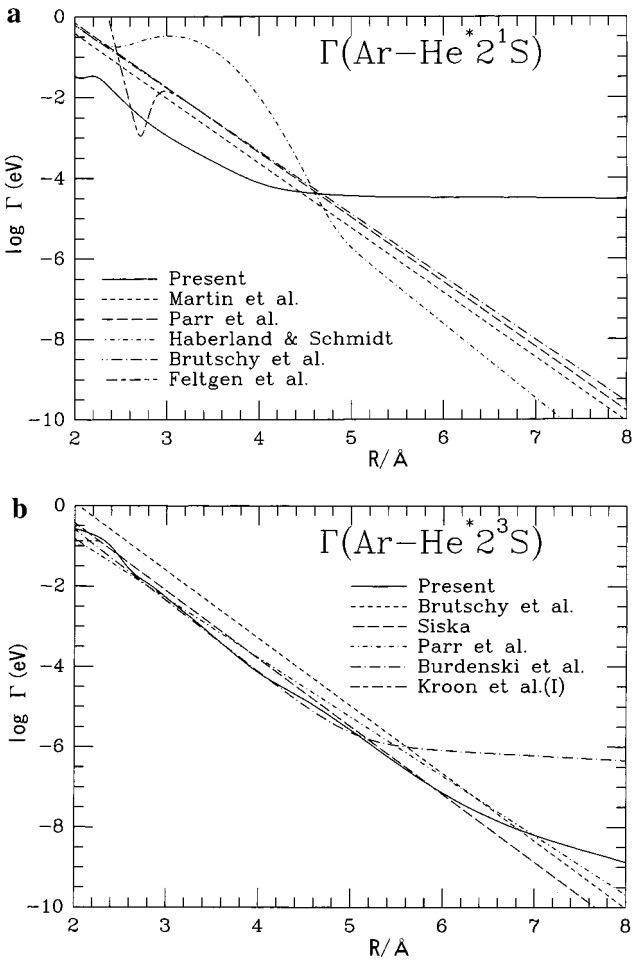

Figure 2. The dependence of total widths Γ on the internuclear distance R for (a) Ar + He*(2^1S) and (b) for Ar + He*(2^3S). The ordinate is in a logalithmic scale. The total widths obtained from experiments by Martin et al.,[13] Parr et al.,[20] Haberland and Smith,[14] Brutschy et al.,[15] and Feltgen et al.[11] are shown for the singlet in part a, and Brutschy et al.,[17] Siska,[18] Parr et al.,[20] Burdenski et al.,[19] and Kroon et al.[21] for the triplet in part b.[48,49] Note that log γ of Feltgen et al. for $R < 3.4$ Å is essentially the same as that of Brutschy et al. in part a, and log γ of Kroon for $R < 2.3$ Å is the same as that of Siska, and their own lines are not drawn in the overlap region to avoid confusion.

shallow minima. A larger CI calculation may reproduce such a shallow minimum.

For the triplet state, the curves obtained by Brutschy et al.,[17] Siska,[18] and Kroon et al.[21] are included in Figure 1b.[49] Burdenski et al.[19] and Parr et al.[20] also proposed different optical potentials, but the real part of their potentials are the same as Siska's. The internuclear distance at the minimum for the present potential is 4.3 Å, and the depth is 36 meV in the present calculation. Experimentally obtained potentials[17,18,21] are close to each other for $V^* < 0.1$ eV relative to the asymptote. Siska reported that the minimum and the depth are 5.2 Å and 5.1 meV,[18] and the values of Brutschy et al. do not seem to be different by very much in this scale. The depth of the minimum is larger in the present calculation. Since the experimentally obtained potential has a very shallow minimum, a quantitative reproduction seems very difficult. The repulsive part of the potential is in good agreement with Siska's potential and width although he used data up to 0.12 eV. Brutschy et al. performed the scattering experiment up to 0.48 eV. Both the potential curves estimated by Brutschy et al. and Kroon et al. have a steeper repulsive part. The change of these potential energy curves (PECs) around $R = 2.8$ Å seems somewhat abrupt in this scale although the PECs were adjusted to fit the experimental result. If more flexible forms for real and imaginary parts of the potential are used, this abrupt change may be reduced.

3.2. Imaginary Parts of Optical Potentials. The dependence of total and partial widths Γ on the internuclear distance R is shown in Figure 2.

See the footnote about the correspondence of the real and imaginary parts.[48]

The decrease of the total width for the singlet channel is less steep than the triplet width, which is due to the existence of the Coulomb-type interaction in the singlet case.[5] The present total widths both for the singlet and triplet states decrease exponentially although the widths show downward deviation at smaller distances and upward deviation at larger distances. Thus, the description by a single-exponential function is worse in these regions. This situation can be seen in other systems.[7,26,27] Nakamura proposed the downward deviation of the width at smaller internuclear distances for the singlet state to explain the energy dependence of the cross section.[50] The width of Haberland and Schmidt[14] is not a single-exponential function, but the behavior of log Γ is rather opposite to ours. Our result for the singlet state indicates that width functions are not single-exponential, but does not support the functional form by Haberland and Schmidt.[14] The width of Feltgen et al. gives the minimum,[11] which was determined to obtain the best fit the

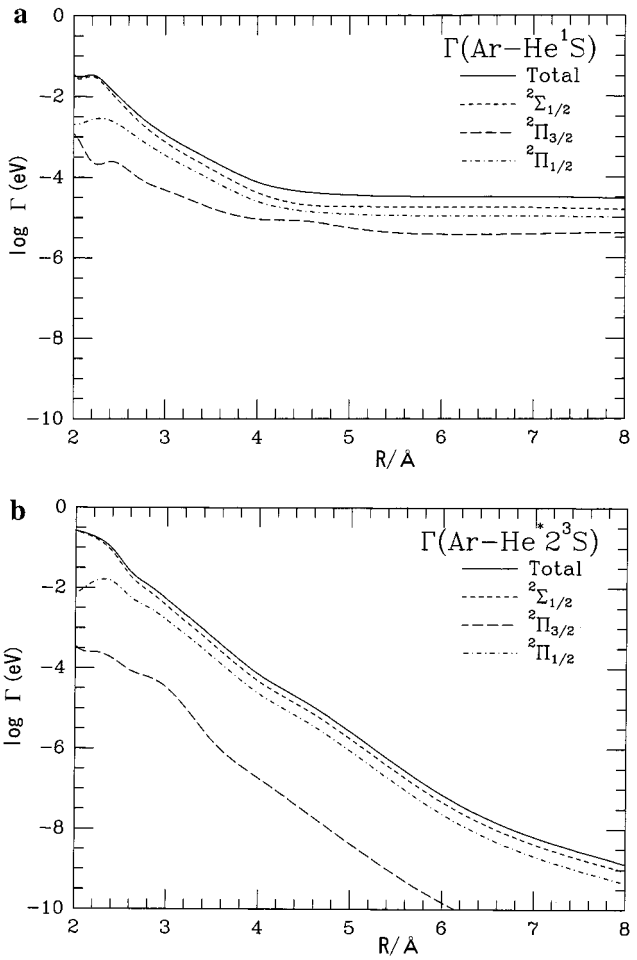

Figure 3. The dependence of the total and partial widths Γ for ArHe$^+$ ($^2\Sigma_{1/2}$, $^2\Pi_{3/2}$, and $^2\Pi_{1/2}$) ionized states on the internuclear distance R for (a) Ar + He*(2^1S) and for (b) Ar + He*(2^3S).

collision energy dependence of the total cross section, but the present result shows no minimum. Feltgen et al. attributed the minimim of their imaginary potential and that of their real potential to the 2s−2p hybridization. However, the occurrence of the minimum would not be due to the hybridization since the present calculation includes both diffuse 2p function in the basis set and the 2p space in the CI space.

For the triplet state in Figure 2b, both the gradient and the magnitude of log Γ for total ionization are in good agreement with those from experiments.[51] Brutschy et al., Burdenski et al., and Siska used a single-exponential function to reproduce their experimental result, but the present curve shows that a deviation from a single-exponential behavior is significant at smaller distances and at larger distances, as for the singlet state. This result is consistent with later evaluation of widths by Burdenski et al. and Kroon et al. Burdenski et al. modified Siska's width to a double-exponential function in order to reproduce their collision energy dependence on total ionization cross section at lower energies.[19] Kroon included this downward deviation in a total width function to explain the energy dependence on the total cross section at higher energies.[21]

Figure 3 shows the calculated total and partial widths which correspond to the ionization into each spin−orbit state for the singlet and triplet species. Both the $^2\Sigma_{1/2}$ and $^2\Pi_{3/2}$ states correlate adiabatically to the $^2P_{3/2}$ state of the Ar^+ ion, and the $^2\Pi_{1/2}$ state correlates to the $^2P_{1/2}$ state. Each state is doubly degenerate. Each partial width decreases exponentially with internuclear distance in R(Ar−He*) = 3−4 Å. At smaller and larger internuclear distances, however, the deviation from the exponential behavior is also clear for each partial width.

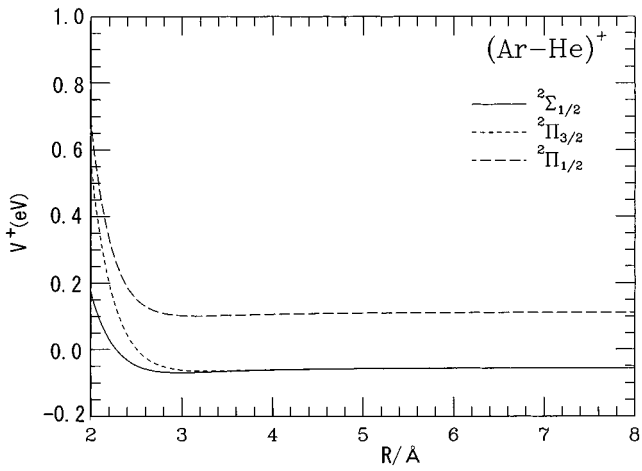

Figure 4. The potential energy curve of ionized states for ArHe$^+$ ($^2\Sigma_{1/2}$, $^2\Pi_{3/2}$, and $^2\Pi_{1/2}$).

The partial widths Γ corresponding to the ionization into the $^2\Sigma_{1/2}$ and $^2\Pi_{1/2}$ states are much larger than that for the $^2\Pi_{3/2}$ state. This is due to the pure Π character of the $^2\Pi_{3/2}$ state. In the Penning ionization of atoms with He *(^1S,^3S), σ-partial waves with respect to the projectile-target axis are dominant, and the widths for ionization into the $^2\Sigma$ states prevail.[52] Thus, the partial widths Γ($^2\Sigma_{1/2}$) and Γ($^2\Pi_{1/2}$) are much larger than Γ($^2\Pi_{3/2}$). Consequently, we may neglect the contribution of this state as pointed out by Longley et al.[8] as a good approximation although the difference for the singlet state is smaller than that for the triplet.

The ratio of Γ($^2\Sigma_{1/2}$) to Γ($^2\Pi_{1/2}$) is two for larger internuclear distances for both the states. This ratio is equal to that of the statistical weight of the correlated $^2P_{3/2}$ to that of the $^2P_{1/2}$ state of Ar^+. At smaller distances, however, the ratios are higher than 2 for both the singlet and triplet states because the $^2\Sigma$-character of Γ($^2\Sigma_{1/2}$) and the Π-character of Γ($^2\Pi_{1/2}$) are dominant.

3.3. Ionized States. Figure 4 shows the potential curves for the spin−orbit ionized states, $^2\Sigma_{1/2}$, $^2\Pi_{1/2}$, and $^2\Pi_{3/2}$. The spin−orbit separation between the ionized Ar $^+$($^2P_{3/2}$) state and Ar $^+$($^2P_{1/2}$) state is calculated to be 0.167 eV, which is comparable to the experimental value, 0.178 eV.[3,4] Gemein and Peyerimhoff carried out an ab initio spin−orbit coupling multireference CI calculation for $HeAr^+$.[53] The present potentials are slightly shallower (14, 12, and 11 meV for $X^2\Sigma_{1/2}$, $A^2\Pi_{3/2}$, and $B^2\Pi_{1/2}$) than theirs (22, 13, and 17 meV) and have larger equilibrium distances (3.0, 3.3, and 3.2 Å) than theirs (2.8, 3.1, and 3.0 Å). The agreement is fairly good although we used one-configuration description for each ionized state.

4. Cross Sections

4.1. Total Ionization Cross Sections. We show the energy dependence of total ionization cross sections in the range of 0.05−1.0 eV in Figure 5.

In Figure 5a the ionization cross section for the singlet state is compared with the results from the optical potentials of other researchers.[11,13,14,20] We did not find absolute cross section measurement results for the singlet state. The optical potentials of Martin et al. and Haberland and Schmidt are obtained from their differential cross section experiments, and seems to include an ambiguity about the magnitude of Γ. The potential of Parr et al. is from a fit to their energy dependence of total ionization cross section, but the cross section is normalized to the room-

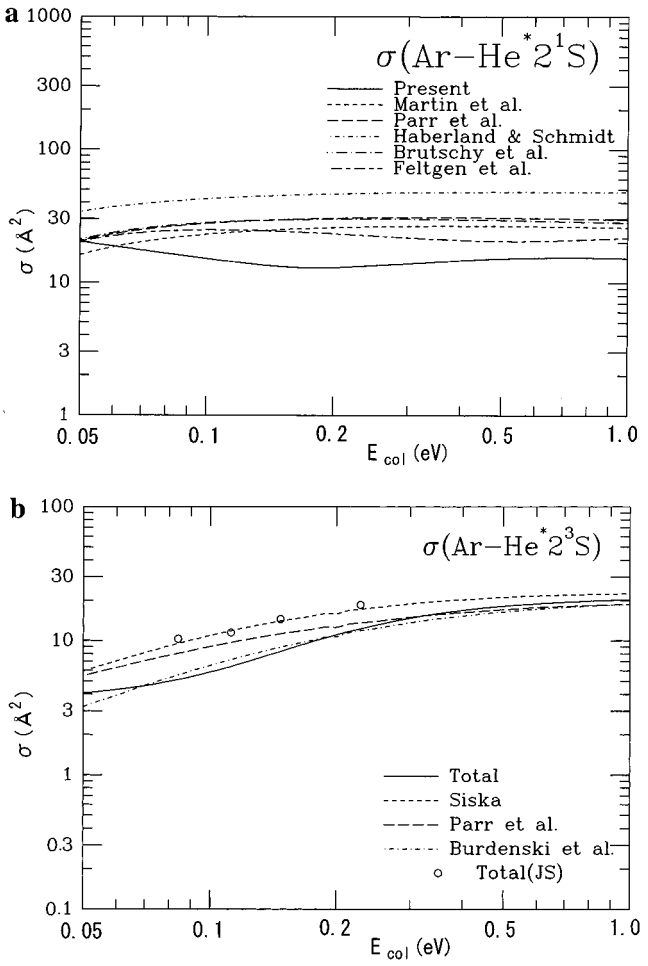

Figure 5. The dependence of ionization cross sections σon collision energy E_{col} for (a) Ar + He*(2^1S) and for (b) Ar + He*(2^3S). In part a, the total ionization cross section by the optical potential obtained by Martin et al.,[13] Parr et al.,[20] Haberland and Smith,[14] and Feltgen et al.[11] are also shown.[48] In part b, the total ionization cross section by the optical potential obtained by Siska,[18] Parr et al.,[20] and Burdenski et al.[19] and the absolute cross section by Jerram and Smith[55] are also shown.

temperature total quenching rate constant in a flowing afterglow experiment.[54] Burdenski et al. also proposed a optical potential that reproduced the energy dependence of ionization cross section, but we did not try to reproduce it because they based it on an unpublished optical potential.[19]

The order of the magnitude of the present cross section is in agreement with that for the other three curves although the present cross section is smaller. The agreement is fair when the ambiguity in the other results is taken into account. The present cross section decreases with collision energy in the energy range of less than 0.2 eV. This is inconsistent with the cross sections of Martin et al. and Haberland and Schmidt, which show a gradual increase with collision energy. This would be due to the upward deviation of the real part potential around 3.0 Å.

For the triplet total ionization cross section in Figure 5b, we also show the curve from the classical calculation with parameters used by Siska,[18] Parr et al.,[20] and Burdenski et al. and several absolute values of total ionization cross section from a velocity-selected metastable atomic beam experiment by Jerram and Smith.[55] Both Parr et al. and Burdenski et al. used Siska's parameters for the real part of the optical potential. Burdenski et al. calculated total cross sections with Siska's parameters for the total width as well as the resonance potential, and found the discrepancy only in lower energies, and modified only the parameters for the width. Parr et al. normalized their experimental curve to a total quenching rate constants,[54] and performed a model calculation with width parameters different from Siska's to get a better fit to their result. This would provide another "experimental" curve for comparison.

The present triplet total width is in good agreement with experimentally obtained cross sections[51] although the agreement for the singlet is fair as discussed above. Superexcited triplet states are probably easier to describe in electronic structure calculations than corresponding singlet states.

The total ionization cross section increases over the energy investigated, and shows saturation at higher energies. This result is in qualitative agreement with the calculation based on parameters experimentally obtained by Siska and other experimental dependences[16,17,19,20,56,57] although the saturation is not clear in some experiments.[16,57] In the lower energy region, the potential well is larger than the collision energy, and the cross section decreases with energy (region I[6,58]). As the energy increases, the collision energy is significantly larger than the potential well, and the repulsive part of the potential plays a predominant role for the behavior of total ionization cross section, which is referred to region II. In region II, the cross section increases. At much higher energies, the cross section starts decreasing again because of probability saturation(region III) although the treatment using the single optical potential may lose significance. The saturation of cross-section increase corresponds to the transition of region II to region III. The energy range investigated of 0.05−1.0 eV falls in region II and region III. In this region, the quantum mechanical interference is not important, so that the classical description is valid as shown above.

4.2. Partial Ionization Cross Sections. Figure 6 shows the total and partial ionization cross sections. The thick lines represent the corresponding quantum mechanical calculation results. For the singlet as well as triplet states, the difference in the total cross section curves is not significant. The classical treatment is, therefore, quite satisfactory in this energy region. The difference in partial cross section curves, however, is clearly seen at higher energies. When partial cross sections are calculated in the quantum mechanical scheme, the sum of the partial cross sections is not equal to the total cross section although this is the case only if partial widths are small enough, which is pointed out in the Calculations section. The results indicate that the sum of the partial ionization cross sections significantly deviates from the total ionization cross section at higher collision energies in quantum dynamics calculations. On the other hand, it is guaranteed that classical total ionization cross section is equal to the sum of partial ionization cross sections from the formalism.

Thus, we conclude that classical treatment for partial cross sections is better and that classical treatment should be used in this energy region (0.05−1 eV) until a consistent quantum mechanical treatment for partial cross section is established.

At lower energies of $E_{col} < 5$ meV, ionization cross sections may show resonance structures.[17,60] However, the resonance structures in integrated ionization cross section have not been observed experimentally so far.

For the triplet state, the partial cross sections for the $^2P_{3/2}$ state and for the $^2P_{1/2}$ state increase. This result is in agreement with the recent experimental results of two-dimensional Penning ionization spectroscopy.[9]

We show the ratio of the calculated partial ionization cross sections in Figure 7. At lower energies, the ratio of the cross

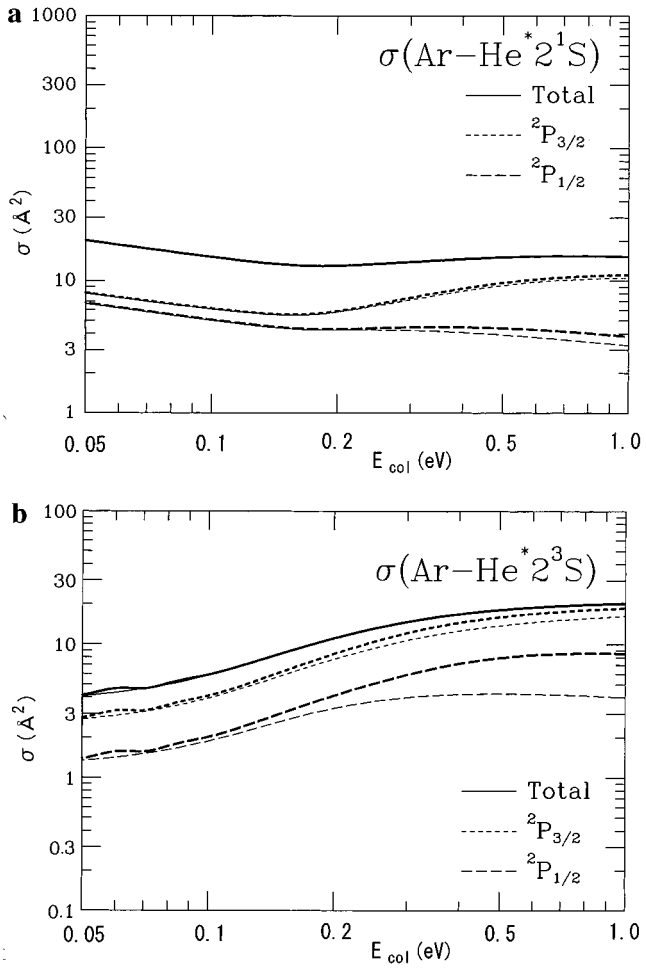

Figure 6. The total cross section and partial cross sections are shown for the calculated width in a classical trajectory calculation(thin curves) and in a quantum mechanical calculation(thick curves) for (a) the singlet and (b) the triplet states.

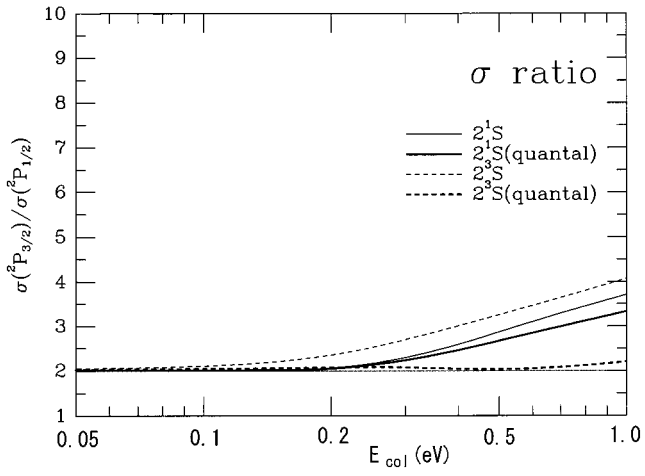

Figure 7. The energy dependence of the ratio of the ionization cross section for the $^2P_{3/2}$ state, $\sigma(^2P_{3/2})$, to that for the $^2P_{1/2}$ state, $\sigma(^2P_{1/2})$. Thin and thick curves are for classical trajectory calculations and quantum mechanical calculations.

section for the $^2P_{3/2}$ state to that for the $^2P_{1/2}(\sigma(^2P_{3/2})/\sigma(^2P_{1/2}))$ is about two, both for the singlet and triplet species. The ratio of the two cross sections at lower energies was two, and this ratio is in agreement with relative electronic state populations in a thermal energy experiment.[61]

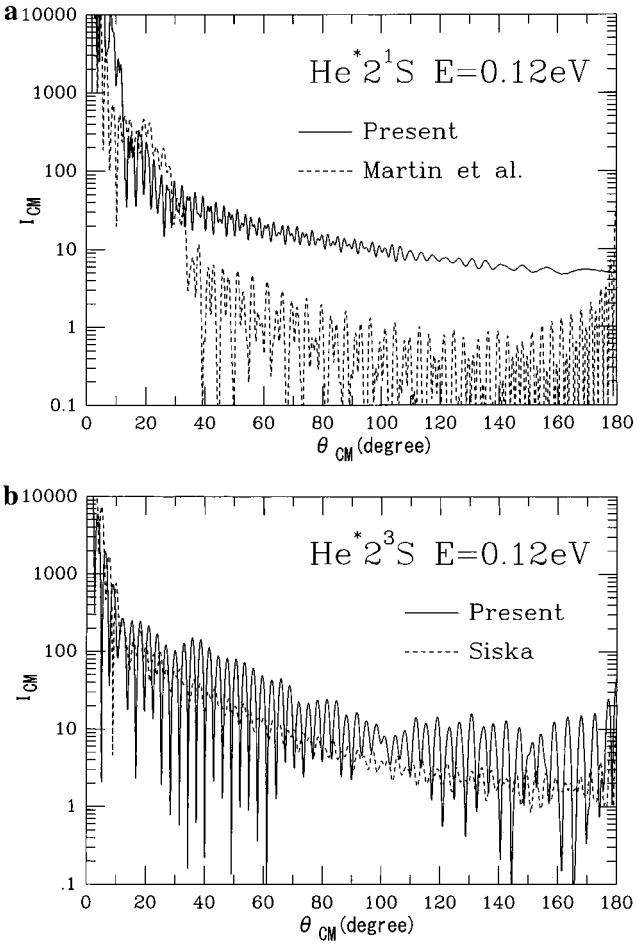

Figure 8. Center-of-mass differential cross sections for Ar−He in the collision energy of 0.12 eV for (a) the singlet and (b) triplet states. The results with the optical potentials by Martin et al.[13] and Siska[18] are included for the singlet and triplet states.

As the collision energy increases, the ratio also increases. On the basis of the classical treatment, the increase for the singlet species is slower than that for the triplet species. The result is in agreement with an early measurement[59] as well as recent two-dimensional Penning ionization spectra.[8,9]

The ratios in quantum mechanical calculations are significantly different from classical results. The quantum treatment underestimated the ratio at higher energies. Furthermore, the increase of the ratio is faster for the singlet state than for the triplet state with collision energy, which is qualitatively inconsistent with the classical result and the experimental measurements. The present results indicate that the quantum mechanical treatment tends to underestimate the ratio of the $\sigma(^2P_{3/2})/\sigma(^2P_{1/2})$ in higher energy regions in similar systems and that classical treatment is desirable to estimate the ratio in the energy range investigated. Longley et al. used a quantum mechanical scheme to obtain the ratio,[8] but the comparison using classical treatment would be desirable.

The collision energy of experimental results has been up to 0.4 eV.[9] The present result predicts at higher energies that the increase of the ratio is more rapid and that the $^2P_{1/2}$ band intensity shows a peak with collision energy.

To analyze the reason for the increase in the ratio, we have examined opacity functions in the previous paper.[31] We investigated ratios of the opacity functions P for several collision energies. Each ratio is the sum of the opacity function for the $^2\Sigma_{1/2}$ state and that for the $^2\Pi_{3/2}$ state to that for the $^2\Pi_{1/2}$ state. The former two states correlate with the $Ar^+(^2P_{3/2})$ state, and

the latter state to the $Ar^+(^2P_{1/2})$ state. The ratio is about two at $E_{col} = 0.05$ eV for all impact parameters, whereas the ratio increases at smaller impact parameters as the collision energy increases. This is clearly because $\Gamma(^2\Sigma_{1/2})$ is more than twice as large as $\Gamma(^2\Pi_{1/2})$ at smaller internuclear distances, which originates in the enhancement of the $^2\Sigma$ character of the $^2\Sigma_{1/2}$ state. Longley et al. also explained the increase of the ratio from the same enhancement for the system $Ar + He(2^1S)$.[8]

4.3. Differential Cross Sections. Figure 8 shows center-of-mass differential cross sections obtained by the quantum mechanical calculation at the collision energy of 0.12 eV. The results for the optical potential obtained by Martin et al.[13] and by Siska[18] are also shown for the singlet and triplet states. For the triplet state, the agreement is reasonable except for quantum mechanical interference. For the singlet state, the present differential cross sections are significantly larger than the results of Martin et al. This is because the real-part of the present potential is more repulsive than that of Martin et al. The agreement with the experiment is not very good for differential cross section even for the triplet state. Differential cross sections may be more difficult to reproduce than the dependence of total and partial ionization cross sections.

5. Summary and Concluding Remarks

Spin−orbit effects on the autoionization from superexcited states of the first kind is examined theoretically for the system $Ar + He^*(2^1S,2^3S) \rightarrow Ar^+(^2P_{3/2},^2P_{1/2}) + He + e^-$. Ab initio calculations have been carried out to obtain the potential energy curves for the entrance and exit channels and partial widths for each spin−orbit ionized state. Classical and quantum dynamics is employed to study the dependence of ionization cross sections on collision energy and angular distribution of the atoms. The calculation has reproduced the order of the ionization cross sections and the experimental fact that the ratio of the cross section for the $^2P_{3/2}$ ionized state to that for the $^2P_{1/2}$ state increases with collision energy for both the singlet and triplet states.

There were arguments about whether an intermediate maximum in the single real-part potential exists or not for the single state. The present ab initio widths indicates that a more flexible form than a single-exponential function should be used for widths to obtain a better fit to experimental results.

Quantum mechanical calculations are shown to underestimate the ratio of $\sigma(^2P_{3/2})/\sigma(^2P_{1/2})$ at higher collision energies. Quantum mechanical calculations are of course exact for the total cross section, but have a flaw in that the sum of partial ionization cross sections is not equal to the total cross section. Thus, a quantum mechanical scheme should be avoided to discuss partial ionization cross sections.

To summarize, the agreement with experiments for the triplet state is good while the agreement for the singlet state is fair. We may need an alternative approach for the singlet state, for example, a filtering method to obtain the optical potential.[62,63]

Acknowledgment. The authors thank the Computer Center, Institute for Molecular Science, Okazaki National Research Institute, for the use of the SP2 workstation cluster system. The present work has been partly supported by Grants in Aid (Grants 12640492 and 12042232) from the Ministry of Education, Science, Sports, and Culture of Japan.

References and Notes

(1) Penning, F. M. *Naturwissenshaften* **1927**, *15*, 818.
(2) Nakamura, H. *Int. Rev. Phys. Chem.* **1991**, *10*, 123.
(3) Turner, D. W.; Baker, C.; Baker, A. D.; Brundle, C. R. *Molecular Photoelectron Spectroscopy*; Wiley-Interscience: London, 1970.
(4) Kimura, K.; Katsumata, S.; Achiba, Y.; Yamazaki, T.; Iwata, S. *Handbook of HeI Photoelectron Spectra of Fundamental Organic Molecules*; Japan Scientific Societies Press: Tokyo, 1981.
(5) Yencha, A. J. in: *Electron Spectroscopy: Theory, Techniques and Applications*; Brundle, C. R., Baker, A. D., Eds.; Academic: London, 1984; Vol. 5, p 196 and references therein.
(6) Ohno, K.; Takami, T.; Mitsuke, K.; Ishida, T. *J. Chem. Phys.* **1991**, *94*, 2675 and references therein.
(7) Siska, P. E. *Mod. Rev. Phys.* **1993**, *65*, 337.
(8) Longley, E. J.; Dunlavy, D. C.; Falcetta, M. F.; Bevsek, H. M.; Siska, P. E. *J. Phys. Chem.* **1993**, *97*, 2097.
(9) Ohno, K.; Yamakado, H.; Ogawa, T.; Yamata, T. *J. Chem. Phys.* **1996**, *105*, 7536.
(10) Longley, E. J.; Siska, P. E. *J. Chem. Phys.* **1997**, *106*, 6365.
(11) Feltgen, R.; Ferkel, H.; Helbing, R. K. B.; Lindinger, A.; Pikorz, D.; Vehmeyer, H. *J. Chem. Phys.* **1999**, *111*, 7298.
(12) Siddiqui, H. R.; Bernfeld, D.; Siska, P. E. *J. Chem. Phys.* **1984**, *80*, 567.
(13) Martin, D. W.; Gregor, R. W.; Jordan, R. M.; Siska, P. E. *J. Chem. Phys.* **1978** *69*, 2833.
(14) Haberland, H.; Schmidt, K. *J. Phys. B* **1977**, *10*, 695.
(15) Brutschy, B.; Haberland, H.; Werner, F. *J. Phys. B* **1982**, *15*, 731.
(16) Pesnelle, A.; Watel, G.; Manus, C. *J. Chem. Phys.* **1975**, *62*, 3590.
(17) Brutschy, B.; Haberland, H.; Schmidt, K. *J. Phys. B* **1976**, *9*, 2693.
(18) Siska, P. E. *Chem. Phys. Lett.* **1979**, *63*, 25.
(19) Burdenski, S.; Feltgen, R.; Lichterfeld, F.; Pauly, H. *Chem. Phys. Lett*. **1981**, *78*, 296.
(20) Parr, T. P.; Parr, D. M.; Martin, R. M. *J. Chem. Phys.* **1982**, *76*, 316.
(21) Kroon, J. P. C.; Senhorst, H. A. J.; Beijerinck, H. C. W. *Chem. Phys*. **1986**, *103*, 119.
(22) Rydberg, R. *Z. Phys.* **1931**, *73*, 326.
(23) Rydberg, R. *Z. Phys.* **1933**, *80*, 514.
(24) Klein, O. *Z. Phys.* **1932**, *76*, 226.
(25) Rees, A. L. G. *Proc. Phys. Soc. London* **1947**, *59*, 998.
(26) Ishida, T. *Chem. Phys. Lett.* **1992**, *191*, 1.
(27) Ishida, T. *J. Chem. Phys.* **1995**, *102*, 4169.
(28) Ishida, T. *Chem. Phys. Lett.* **1993**, *211*, 1.
(29) Ishida, T. *J. Chem. Phys.* **1996**, *105*, 1392.
(30) Ishida, T.; Horime, K. *J. Chem. Phys.* **1996**, *105*, 5380.
(31) Ishida, T.; Katagiri, H. *Chem. Phys. Lett.* **1997**, *274*, 293.
(32) Feshbach, H. *Ann. Phys. (New York)* **1958**, *5*, 357; **1962**, *19*, 287.
(33) Hickman, A. P.; Isaacson, A. D.; Miller, W. H. *J. Chem. Phys.* **1977**, *66*, 1492.
(34) Takahashi, T.; Mori, M. *Publication RIMS*; Kyoto University: Kyoto, 1974; Vol. 9, p 721.
(35) Vellerling, W. T.; Teukolsky, S. A.; Press, W. H.; Flannery, B. P. *Numerical Recipes*, Cambridge University Press: New York, 1992.
(36) King, H. F.; Furlani, T. R. *J. Comput. Chem.* **1988**, *9*, 771.
(37) Dupuis, M.; Watts, J. D.; Villar, H. O.; Hurst, G. J. B. *Quantum Chemistry Program HONDO7*.
(38) For example, Hecht, H. G.; *Mathematics in Chemistry. An Introduction to Modern Method*; Prentice Hall: New York, 1990.
(39) Nakamura, H. *J. Phys. Soc. Jpn.* **1969**, *26*, 773.
(40) Miller, W. H. *J. Chem. Phys.* **1970**, *52*, 3563.
(41) Cohen, J. S.; Lane, N. F. *J. Chem. Phys.* **1977**, *66*, 586.
(42) Johnson, B. R. *J. Comput. Phys.* **1973**, *13*, 445.
(43) Brutschy, B.; Haberland, H.; Morgner, H.; Schmidt, K. *Phys. Rev. Lett.* **1976**, *36*, 1299.
(44) Alpeter, R.; Haberland, H.; Konz, W.; Oesterlin, P.; Schmidt, K. *J. Chem. Phys.* **1977**, *67*, 836.
(45) Haberland, H.; Lee, Y. T.; Siska, P. E. *Adv. Chem. Phys.* **1981**, *47*, 487.
(46) Jordan, R. W.; Martin, D. W.; Siska, P. E. *J. Chem. Phys.* **1978**, *69*, 2833.
(47) Haberland, H.; Oesterlin, P. *Z. Phys. A.* **1981**, *304*, 11.
(48) Parr et al.[20] and Burdenski et al.[19] used the same real part of the optical potential as Siska's.[18] Feltgen proposed several functional forms, and they obtained the best fit using the real part of Brutchy et al. for the singlet state and the imaginary part Γ_p in ref 11. Thus, we included Γ_p in Figure 2a.
(49) Kroon, et al. proposed two optical potentials. Each of the optical potentials uses a different pair of the real part and the imaginary part, and they concluded that optical potential I is preferable. Thus, we include only potential I. In the curve of Brutschy et al., there are two discontinuity at 2.43 and 2.65 Å, which may come from a small significant digit in their parameters.[17]
(50) Nakamura, H. *J. Phys. B* **1976**, *9*, L59.

(51) In ref 31, the magnitude was underestimated because the statistical factor of 3 for the triplet state was not taken into account. In Figure 2 of ref 31, all the curves except for total (Siska) should have been shifted upward by log 3 = 0.477.
(52) Morgner, H. *Comments At. Mol. Phys.* **1982**, *11*, 271.
(53) Gemein, B.; Peyerimhoff, S. D. *Chem. Phys. Lett*. **1990**, *173*, 7.
(54) Schmeltekopf, A. L.; Fehsenfeld, F. C. *J. Chem. Phys.* **1970**, *53*, 3173.
(55) Jerram, P. A.; Smith, A. C. H. *J. Phys. B* **1985**, *18*, 1747.
(56) Illenberger, E.; Niehaus, A. *Z. Phys. B* **1975**, *20*, 33.
(57) Woodard, M. R.; Sharp, R. C.; Seely, M.; Muschlitz, E. E., Jr. *J. Chem. Phys.* **1978**, *69*, 2978.
(58) Nakamura, H. *J. Phys. B* **1975**, *L489*, 8.
(59) Hotop, H.; Kolb, E.; Lorenzen, J. *J. Electron Spectrosc.* **1979**, *16*, 213.
(60) Olson, R. E. *Phys. Rev. A* **1972**, *6*, 1031.
(61) Brion, C. E.; McDowell, C. A.; Stewart, W. B. *J. Electron Spectrosc. Relat. Phanom.* **1972/73**, *1*, 113.
(62) Neuhauser, D. *J. Chem. Phys.* **1990**, *93*, 2611.
(63) Takatsuka, K.; Hashimoto, N. *J. Chem. Phys.* **1995**, *103*, 6057.